ACS OMEGA

Open Access

http://pubs.acs.org/journal/acsodf

Article

Emissive Alkylated Guanine Analogs as Probes for Monitoring O^6-Alkylguanine-DNA-transferase Activity

Kfir B. Steinbuch,[‡] Marcela Bucardo,[‡] and Yitzhak Tor*

Cite This: *ACS Omega* 2024, 9, 36778−36786

Read Online

ACCESS | Metrics & More | Article Recommendations | Supporting Information

ABSTRACT: Human O^6-alkylguanine-DNA-transferase (hAGT) is a repair protein that provides protection from mutagenic events caused by O^6-alkylguanine lesions. As this stoichiometric activity is tissue-specific, indicative of tumor status, and correlated to chemotherapeutic success, tracking the activity of hAGT could prove to be informative for disease diagnosis and therapy. Herein, we explore two families of emissive O^6-methyl- and O^6-benzylguanine analogs based on our previously described $^{th}G_N$ and $^{tz}G_N$, thieno- and isothiazolo-guanine surrogates, respectively, as potential reporters. We establish that O^6-Bn$^{th}G_N$ and O^6-Bn$^{tz}G_N$ provide a spectral window to optically monitor hAGT activity, can be used as substrates for the widely used SNAP-Tag delivery system, and are sufficiently bright to be visualized in mammalian cells using fluorescence microscopy.

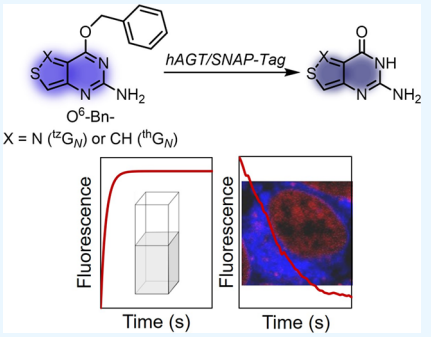

INTRODUCTION

DNA alkylation can be caused by both endogenous and exogenous agents.[1,2] Cellular repair mechanisms exist to evade the potentially mutagenic outcomes from such nucleobase modifications, thus maintaining genome integrity.[3,4] Human O^6-alkylguanine-DNA-transferase (hAGT) is a repair protein that protects DNA from O^6-alkylguanine lesions.[5,6] Mechanistically, hAGT acts by irreversibly transferring an alkyl group from the O6 position of the alkylated guanine to a cysteine residue to form a stable thioether and restore the native purine.[7] hAGT thus is a suicide protein, meaning that each repair event tags the protein for degradation.[8] Although the O6 alkylation of guanine is not the most common guanine modification, hAGT's stoichiometric reaction suggests a highly important protective activity.[8]

The cellular activity of hAGT has been associated with disease progression and therapeutic susceptibility of various cancers.[9,10] Classical chemotherapeutic agents alkylate DNA, causing cytotoxicity, implying potential resistance if hAGT activity is upregulated.[11] Glioblastoma, for example, the most common type of malignant brain tumor, is treated with temozolomide, a methylating agent.[12] Its efficacy is diminished, however, with elevated hAGT activity.[13] As hAGT activity is tissue-dependent and varies with disease progression, having a simple and real-time fluorescence-based detection to measure its activity, including in live cells, could prove useful.[14] While some fluorescence-based methods have previously been described (including one utilizing $^{th}G_N$),[15] emphasizing the significance and necessity of such assays,[15,16] many of these methods are multistep and complex.[17−19]

In addition to its native roles, hAGT was engineered to function as a highly specific protein self-labeling tag, coined SNAP-Tag.[20] By adorning the benzyl moiety of O^6-benzylguanine with an emissive dye, for example, the SNAP-Tag and a genetically fused protein can be labeled for diverse biotechnological applications.[20−22]

Our lab has developed two fluorescent RNA alphabets based on the thieno[3,4-*d*]pyrimidine (^{th}N) and isothiazolo[4,3-*d*]pyrimidine (^{tz}N) heterocyclic cores (Figure 1a).[23,24] Their

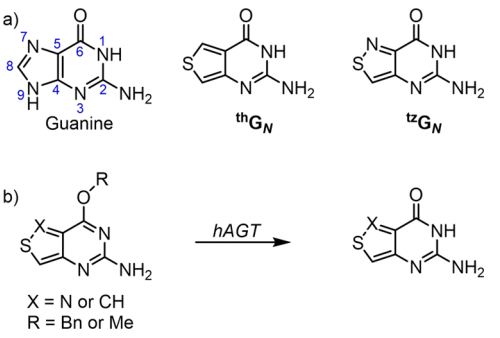

Figure 1. (a) Structures of guanine (displaying the conventional purine numbering system), as well as $^{th}G_N$ and $^{tz}G_N$. (b) Potential conversion of O^6-alkylguanine analogs (O^6-Bn$^{th}G_N$ and O^6-Me$^{th}G_N$ or O^6-Bn$^{tz}G_N$ and O^6-Me$^{tz}G_N$) to the respective guanine analogs ($^{th}G_N$ or $^{tz}G_N$) by hAGT.

Received: June 18, 2024
Revised: July 22, 2024
Accepted: August 13, 2024
Published: August 17, 2024

isomorphic character provides biochemically active nucleoside surrogates, which are endowed with useful photophysical features that are absent in their native counterparts. These compounds have served as powerful biophysical tools for exploring cellular processes involving nucleosides, nucleotide cofactors, and secondary messengers.[25,26] Specifically, the emissive guanine analogs were previously utilized to monitor the activity of human guanine deaminase.[27] We therefore set to investigate the substrate recognition of hAGT with the thieno, O^6-BnthG$_N$ and O^6-MethG$_N$, and isothiazolo, O^6-Bn^{tz}G$_N$ and O^6-Me^{tz}G$_N$, O^6-alkylguanine analogs (Figure 1b; note the nomenclature and numbering comment in the caption).

Here, we describe the synthetic methods explored to activate the previously published thG$_N$[23] and ^{tz}G$_N$[24] at their respective O6 positions (Figure 1). The photophysical properties of the alkylated guanine analogs were then characterized, and the tolerance of hAGT to the alkyl guanine surrogates was investigated. To further exemplify the value of these analogs, their ability to monitor reactions by SNAP-Tag and their utility for live-cell imaging in mammalian cells were studied. We found that both benzylated nucleobases O^6-BnthG$_N$ and O^6-Bn^{tz}G$_N$ provide a spectral window to optically monitor hAGT activity and can be used as substrates for the widely used SNAP-Tag delivery system. Additionally, both benzylated derivatives showed uptake by mammalian cells and were sufficiently bright for cellular visualization by fluorescence microscopy. These findings therefore present a simple and direct method to fluorescently monitor hAGT in vitro and potentially visualize its activity in live cells.

RESULTS AND DISCUSSION

Emissive guanine analogs containing either a thienopyrimidine core, thG$_N$, or an isothiazolopyrimidine core, ^{tz}G$_N$, were prepared according to previously reported procedures.[23,24] Briefly, either the commercially available methyl 4-amino-thiophene 3-carboxylate hydrochloride or in-house synthesized 4-aminoisothiazole-3-carboxamide hydrochloride[28] was cyclized with chloroformamidine hydrochloride in $DMSO_2$ at 125 °C to yield thG$_N$ or ^{tz}G$_N$, respectively. These core structures served as the starting materials for synthesizing the O^6-alkylated guanine analogs.

The alkylated guanine surrogates of interest were the O^6-benzyl derivatives, as O^6-benzylguanine is the most favorable substrate for hAGT and the specific substrate engineered for the SNAP-Tag protein,[20] and the O^6-methyl derivatives, as methylated G is the most biologically relevant alkylated guanine.[5,11] Classically, such derivatives have been prepared via a Mitsunobu reaction.[29] In the case of our thienopyrimidine and isothiazolopyrimidine heterocycles, however, Mitsunobu reactions yielded mixtures of N^1-, exo N^2-, and only traces of O^6-alkylated thienopyrimidine products or only N^1- and exo N^2-alkylated isothiazolopyrimidine products, respectively (note, for simplicity, that the conventional numbering of the purine system is used as shown in Figure 1; see SI, Section S2 for crystal structures). Alternative reported methods[15,30] were thus employed, as summarized for the O^6-benzyl derivatives in Scheme 1 and O^6-methyl derivatives in Schemes S1 and S2. To activate thG$_N$ at its carbonyl, benzotriazole-1-yloxytris-(dimethylamino)phosphonium hexafluorophosphate (BOP) and DBU were used followed by the addition of 0.5 M sodium benzyloxide in benzyl alcohol or 1 M sodium methoxide in methanol to afford O^6-BnthG$_N$ (see SI, Section S2 for crystal structures) and O^6-MethG$_N$ in 64 and 86% yields,

Scheme 1. Synthesis of O^6-Benzyl Thieno- and Isothiazolo-guanine Analogs

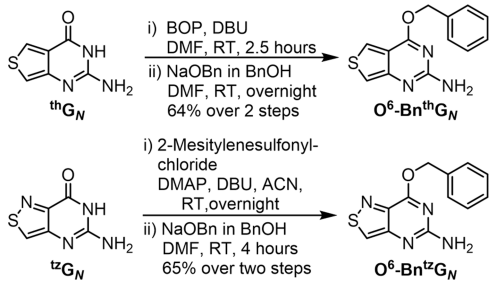

respectively. To produce the isothiazolopyrimidine derivatives, ^{tz}G$_N$ was activated by producing a DMAP−^{tz}G$_N$ salt using DMAP, 2-mesitylenesulfonyl, and DBU and then exposing the activated salt to 0.5 M sodium benzyloxide in benzyl alcohol or 1 M sodium methoxide in methanol, to yield O^6-Bn^{tz}G$_N$ and O^6-Me^{tz}G$_N$ in 65 and 75% yields, respectively (Scheme 1 and S2).

To evaluate whether the alkylated nucleobases (i.e., the enzyme's substrate) and the corresponding parent heterocycles (i.e., the product) are photophysically distinguishable, their spectroscopic properties were evaluated in water (Figure 2a).

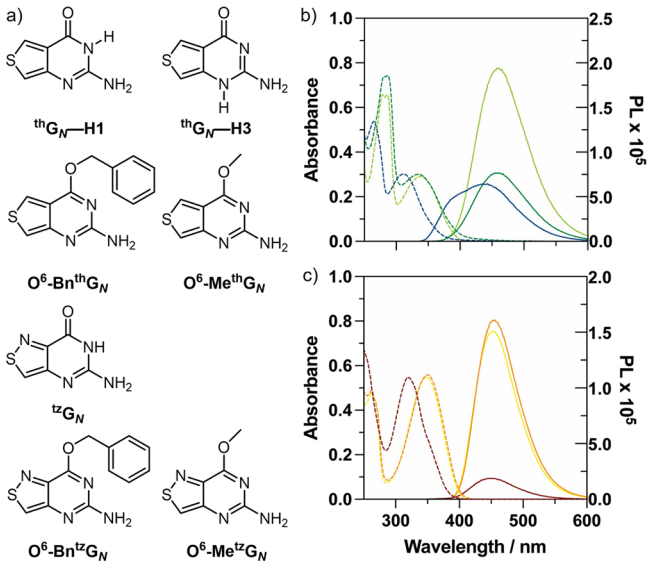

Figure 2. (a) Structures of thG$_N$-H1, thG$_N$-H3, O^6-BnthG$_N$, O^6-MethG$_N$, ^{tz}G$_N$, O^6-Bn^{tz}G$_N$, and O^6-Me^{tz}G$_N$ nucleobase analogs. (b) Absorption (dashed lines) and emission (solid lines) of thG$_N$ (blue), O^6-BnthG$_N$ (dark green), and O^6-MethG$_N$ (lime). (c) Absorption (dashed lines) and emission (solid lines) of ^{tz}G$_N$ (red), O^6-Bn^{tz}G$_N$ (orange), and O^6-Me^{tz}G$_N$ (yellow).

As seen in Figure 2b,c and summarized in Table 1, the absorption and emission spectra of the two heterocyclic families show substantial shifts when alkylated and offer a means to distinguish substrates from reaction products. The guanine analogs, thG$_N$ and ^{tz}G$_N$, were previously shown to have bathochromically shifted absorption and emission maxima when compared to guanine in water (λ_{max} of 315 and 320 nm, $\lambda_{em,max}$ of 439 and 446 nm, respectively).[27] The O-alkylation caused additional redshifting for both heterocyclic families, showing absorption maxima at 337, 338, 350, and 349 nm for O^6-BnthG$_N$, O^6-MethG$_N$, O^6-Bn^{tz}G$_N$, and O^6-Me^{tz}G$_N$, respec-

https://doi.org/10.1021/acsomega.4c05700
ACS Omega 2024, 9, 36778−36786

Table 1. Photophysical Data of Nucleobase Analogs in Water

	$\lambda_{abs,max}$ [a]	ε [b]	$\lambda_{em,max}$ [a]	ϕ	$\varepsilon\phi$
$^{th}G_N$ [c]	315	3.0 ± 0.1	439	0.40 ± 0.04	1200
O^6-Bn$^{th}G_N$	337	3.2 ± 0.02	460	0.42 ± 0.01	1344
O^6-Me$^{th}G_N$	338	3.1 ± 0.03	465	0.85 ± 0.01	2635
$^{tz}G_N$ [c]	320	5.4 ± 0.1	446	0.07 ± 0.01	378
O^6-Bn$^{tz}G_N$	350	5.8 ± 0.02	460	0.83 ± 0.01	4814
O^6-Me$^{tz}G_N$	349	5.6 ± 0.03	459	0.83 ± 0.01	4648

[a] $\lambda_{abs,max}$ and $\lambda_{em,max}$ are in nm. [b] ε is in 10^3 M^{-1} cm^{-1}. Measured in triplicate in water. [c] Previously reported values.[27]

tively. Similarly, fluorescence spectroscopy shows substantial changes that provide different photophysical fingerprints for each derivative, with emission maxima at 460, 465, 460, and 459 nm for O^6-Bn$^{th}G_N$, O^6-Me$^{th}G_N$, O^6-Bn$^{tz}G_N$, and O^6-Me$^{tz}G_N$, respectively (Figure 2).

All derivatives, excluding $^{th}G_N$, exhibit classically shaped emission bands (Figure 2b,c). In contrast, the thiophenopyrimidine $^{th}G_N$ analog populates two tautomeric forms in H-bonding-capable solvents, such as water, and displays a blueshifted shoulder.[23] Spectral deconvolution of the absorption and emission spectra has previously shown that each tautomer can be selectively excited.[31] The long and short emitting tautomers have been attributed to the $^{th}G_N$-1H and $^{th}G_N$-3H keto-amino tautomers, respectively (Figure 2a).[31] Once $^{th}G_N$ is alkylated at the O6 position, the structure is locked into one favorable tautomeric form, thus displaying only a redshifted emission band. Additionally, all alkylated products possess a higher emission quantum yield compared to their parent nonalkylated heterocycles. O^6-Bn$^{th}G_N$ displayed a small increase to 0.42 from 0.40 of the nonalkylated precursor $^{th}G_N$, while O^6-Me$^{th}G_N$ showed a substantial increase to 0.85 (Figure 2b and Table 1). Both O^6-Bn$^{tz}G_N$ and O^6-Me$^{tz}G_N$ showed much higher emission quantum yields compared to the nonalkylated precursor $^{tz}G_N$ (ϕ = 0.83 and 0.07, respectively; Figure 2c and Table 1). The alkylated derivatives portray comparable molar absorptivity to the nonalkylated parent molecule; however, the increase in emission quantum yield observed for O^6-Me$^{th}G_N$, O^6-Bn$^{tz}G_N$, and O^6-Me$^{tz}G_N$ consequently produces a substantial increase in apparent brightness (Table 1). The brightness thus increases over 2-fold for O^6-Me$^{th}G_N$ compared to $^{th}G_N$ and over 4-fold for O^6-Bn$^{tz}G_N$ and O^6-Me$^{tz}G_N$ compared to $^{tz}G_N$.

To test the alkylated derivatives as hAGT and SNAP-Tag substrates and assess their utility in tracking dealkylation reactions, they were subjected to the corresponding commercially available recombinant proteins. The reactions were run in a DPBS buffer at 37 °C and monitored by fluorescence spectroscopy via excitation at the isosbestic point of each pair of compounds under the same conditions. Given the different spectroscopic characteristics of the alkylated vs the nonalkylated parent heterocycles, tracking of the substrate to product conversion should show a time-dependent change in emission.

Rewardingly, O^6-Bn$^{th}G_N$ and O^6-Bn$^{tz}G_N$ show a change in the emission intensity at a single wavelength when exposed to hAGT. An increase in the emission at 400 nm is seen for O^6-Bn$^{th}G_N$ (Figure 3a). This increase is consistent with its transformation to $^{th}G_N$, and the emission signal associated with the short emitting tautomer is unavailable to the locked reaction substrate. A decrease in emission at 450 nm is seen for

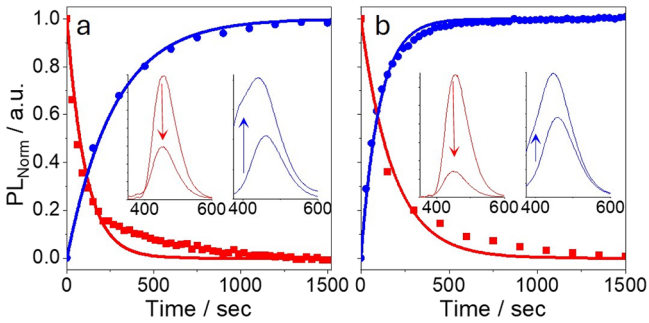

Figure 3. Data and curve fits of normalized fluorescence changes upon dealkylation of O^6-Bn$^{th}G_N$ to $^{th}G_N$ at 400 nm (blue) and O^6-Bn$^{tz}G_N$ to $^{tz}G_N$ at 450 nm (red) by (a) hAGT and (b) SNAP-Tag. Data presented are the averages of three independent experiments. For normalized data with error bars, see Figure S5. Insets: Before and after emission spectra for O^6-Bn$^{th}G_N$ (blue) and O^6-Bn$^{tz}G_N$ (red) reactions. Arrows show the observed change at the monitored wavelength.

O^6-Bn$^{tz}G_N$, consistent with transformation to the less bright $^{tz}G_N$ (Figure 3a). No significant emission changes were observed for O^6-Me$^{th}G_N$ and O^6-Me$^{tz}G_N$ within the tested time windows (Figure S5). This can potentially be rationalized by the innate preference of the hAGT protein for O^6-BnG$_N$ over O^6-MeG$_N$ as reported.[20] Reaction $t_{1/2}$ values were calculated assuming a pseudo-first-order reaction kinetics for the dealkylation of both benzylated analogs to the corresponding "repaired" thiophenopyrimidine or isothiazolepyrimidine nucleobase ($t_{1/2}$ = 173 and 77 s for O^6-Bn$^{th}G_N$ and O^6-Bn$^{tz}G_N$, respectively; Table 2). These $t_{1/2}$ values are 4 and 9 times

Table 2. hAGT and SNAP-Tag Reaction Rates

		hAGT		SNAP-Tag	
	λ_{exc} [a]/λ_{mntr} [a]	k_{app} [b]	$t_{1/2}$ [c]	k_{app} [b]	$t_{1/2}$ [c]
O^6-Bn$^{th}G_N$ to $^{th}G_N$	321/400	0.004 ± 7 × 10^{-5}	173 ± 3	0.010 ± 2 × 10^{-4}	69 ± 1
O^6-Me$^{th}G_N$ to $^{th}G_N$	325/400	--[d]	--[d]	--[d]	--[d]
O^6-Bn$^{tz}G_N$ to $^{tz}G_N$	334/450	0.009 ± 4 × 10^{-4}	77 ± 3	0.005 ± 4 × 10^{-4}	139 ± 10
O^6-Me$^{tz}G_N$ to $^{tz}G_N$	334/450	--[d]	--[d]	--[d]	--[d]
O^6-R-BnG$_N$ to G$_N$	-	1 × 10^{-3}[e]	7 × 10^{2}[e]	-	-
O^6-BnG$_N$-Cy3 to G$_N$	-	-	-	5 × 10^{-2}[f]	13[f]

[a] λ_{exc} and λ_{mntr} are reported in nm and represent the wavelength for excitation and wavelength monitored, respectively. [b] k_{app} pseudo-first-order rate constant reported in s^{-1}. [c] Reaction half-life calculated assuming pseudo-first-order kinetics, reported in s. Experiments done in triplicate. [d] No significant fluorescence changes were seen within the time window tested (Figure S5). [e] Values calculated based on reported values from ref 20. [f] Values calculated based on reported values from ref 32. See SI, Section S5 for more details.

shorter than the $t_{1/2}$ calculated for O^6-BnG$_N$ from previously reported values (SI, Section S5).[20] This suggests that the fluorescent alkylated guanine surrogates presented here are more effective substrates for hAGT than native benzylated guanine.

To preliminary demonstrate the utility of the alkylated analogs in the context of real-time protein fluorescence labeling or cargo delivery using the SNAP-Tag technology, the

https://doi.org/10.1021/acsomega.4c05700
ACS Omega 2024, 9, 36778−36786

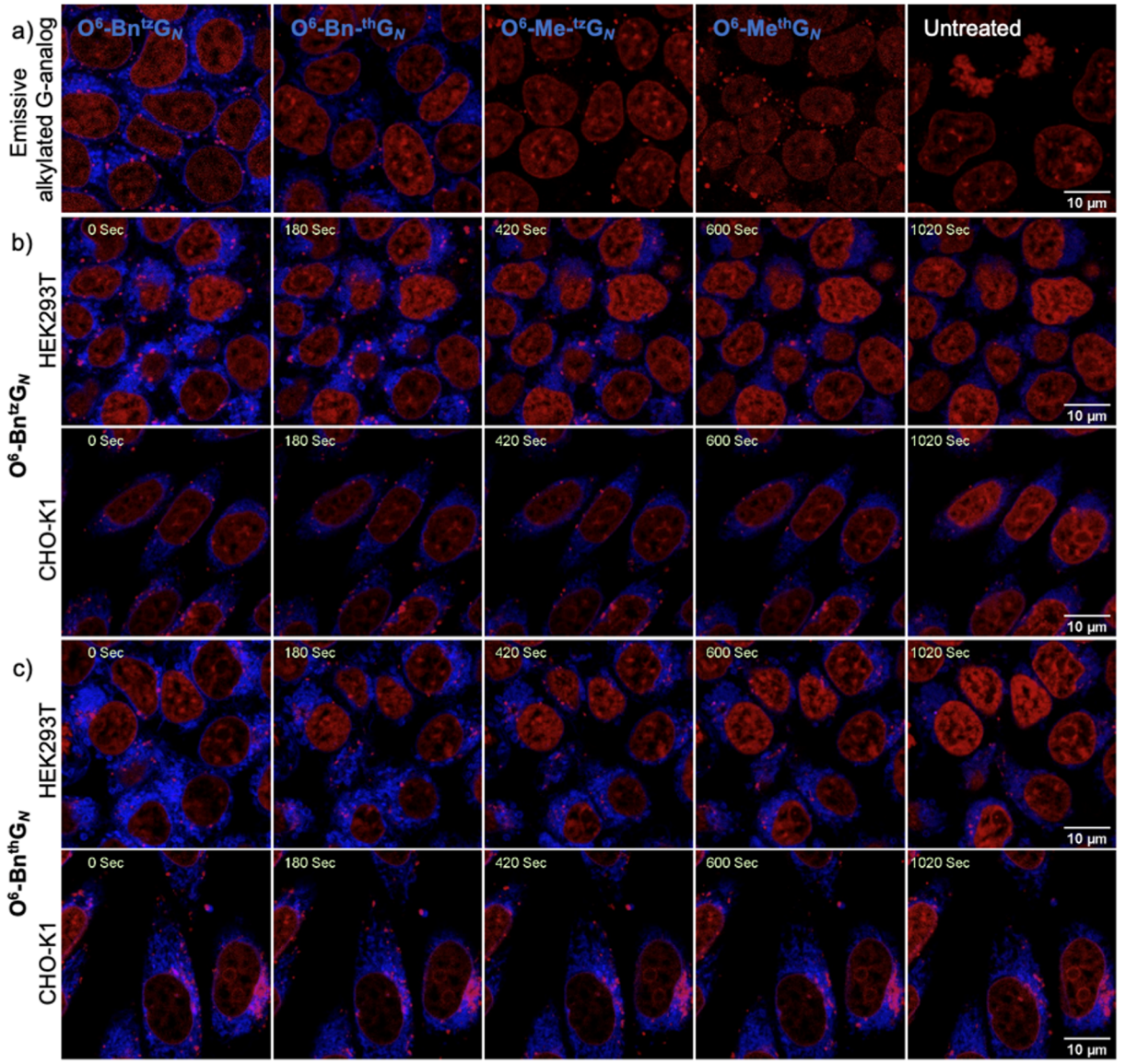

Figure 4. (a) Live-cell imaging of O^6-$Bn^{th}G_N$, O^6-$Me^{th}G_N$, O^6-$Bn^{tz}G_N$, and O^6-$Me^{tz}G_N$ in HEK293T cells after 1 h of incubation versus untreated cells. (b) Fluorescence images of HEK293T cells and CHO-K1 cells incubated with 500 μM O^6-$Me^{tz}G_N$ and (c) 100 μM O^6-$Bn^{th}G_N$ at indicated times. Cells' nuclei were visualized using NucRed.

emission intensity was monitored using the same protocol as for hAGT but with the commercially available purified SNAP-Tag protein. Similar to reactions with hAGT, the resulting photophysical data showed that the reactions of O^6-$Bn^{th}G_N$ and O^6-$Bn^{tz}G_N$ are accompanied by a detectable change in emission intensity (Figure 3b). Incubation with O^6-$Me^{th}G_N$ and O^6-$Me^{tz}G_N$ did not show, again, a significant change in emission (Figure S5). Reaction $t_{1/2}$ values were calculated for the reactions with the SNAP-Tag protein ($t_{1/2}$ = 69 and 139 s for O^6-$Bn^{th}G_N$ and O^6-$Bn^{tz}G_N$, respectively, see Table 2). These values are about 5 and 10 times longer than the $t_{1/2}$ calculated for O^6-BnG_N, which is consistent with the fact that the SNAP-Tag was specifically "evolved" to dealkylate O^6BnG_N.[32] While these values nicely correlate with our observations, we caution that they provide only an approximation.

The changes in emission intensity observed with O^6-$Bn^{th}G_N$ and O^6-$Bn^{tz}G_N$ (Figure 3) are consistent with the dealkylation reaction of these substrates with both hAGT and SNAP-Tag. Notably, O^6-$Bn^{tz}G_N$ displays a faster reaction with hAGT than O^6-$Bn^{th}G_N$, showcasing the increased functionality of the isothiazolopyrimidine analogs, which possess a nitrogen atom in a position equivalent to the N7 position in native nucleobases and nucleosides. Previous explorations have shown necessary interactions of the protein with the nucleobase's N7, O6, N3, and its heterocyclic amine, while substitutions at the C8 and N9 positions are tolerated.[33−36] Such enzyme−substrate interactions are not disrupted by the isothiazolo analogs reported here.

Intriguingly, the relative reaction rates for O^6-$Bn^{th}G_N$ and O^6-$Bn^{tz}G_N$ with the SNAP-Tag protein were reversed, compared to hAGT. This is likely resulting from the engineering of the SNAP-Tag protein.[20,21] From the library of hAGT mutants tested for increased activity and selectivity for benzylated guanosine derivatives, protein mutants containing S159E showed increased efficiency.[20,21] In hAGT, Ser159 may act as a hydrogen bond donor to the basic N7 site.[20,34] In the SNAP-Tag protein, it is mutated to glutamic acid, which is

https://doi.org/10.1021/acsomega.4c05700
ACS Omega 2024, 9, 36778−36786

deprotonated, and the reactive substrate is tautomerized to N7−H instead of the N9−H.[32,37] Such tautomerization is not possible for the thiopheno and isothiazolo analogs. However, the hydrogen at the thiophene's C7 position can potentially be better accommodated by the deprotonated glutamic acid residue.[33] Additionally, we note a higher reactivity for the benzylated analogs, which react efficiently with both hAGT and the SNAP-Tag, while the methyl alkylated analogs do not. This is consistent with previously published data regarding their substrate reactivity.[33]

To substantiate the fluorescently monitored enzymatic conversion of O^6-BnthG$_N$ and O^6-Bn^{tz}G$_N$ to thG$_N$ and ^{tz}G$_N$, their respective nucleobases, and to assess the reactions' completion, the conversions were monitored by HPLC at $t = 0$ and 1500 s (Figures S2 and S3). Chromatographic analyses and comparison to authentic samples demonstrated full consumption of both O^6-BnthG$_N$ and O^6-Bn^{tz}G$_N$ and the formation of the corresponding nucleobases thG$_N$ and ^{tz}G$_N$, respectively, by both hAGT and SNAP-Tag (Figures S2 and S3).

A preliminary HPLC-monitored competition reaction containing 1 equiv each of O^6-Bn^{tz}G$_N$, O^6-BnthG$_N$, and the native O^6-BnGN, set for 80 s (ca. $t_{1/2}$ of O^6-Bn^{tz}G$_N$), has shown the consumption of O^6-Bn^{tz}G$_N$ and O^6-BnthG$_N$ by hAGT and no consumption of O^6-BnG$_N$. This is in agreement with the $t_{1/2}$ values listed in Table 2 and further suggests that the emissive benzylated analogs are more effective substrates for hAGT than O^6-BnG$_N$ (Figure S4). A similar 60 s competition reaction was executed for the SNAP-Tag as well. HPLC illustrated partial consumption of all three substrates (including O^6-BnG$_N$) aligned, again, with the kinetic values obtained (Figure S4).

Following the HPLC and fluorescence-based kinetic evaluation of substrate recognition by hAGT and SNAP-Tag, we sought to evaluate whether the chromophoric features of these emissive alkylated guanine surrogates could be utilized for live-cell imaging in mammalian cells. O^6-BnthG$_N$, O^6-MethG$_N$, O^6-Bn^{tz}G$_N$, and O^6-Me^{tz}G$_N$ were added to human embryonic kidney (HEK293T) cells, which are known to express substantial amounts of cytosolic hAGT.[16] After a calibration experiment to determine the working concentration range on an EVOS widefield fluorescence microscope (Figures S6 and S9), cells were incubated with the thiopheno analogs (100 μM) and the isothiazolo analogs (500 μM) for 1 h. For visualization purposes, cultures were also incubated with the live-cell nuclear dye NucRed for the last 30 min of the incubation time. Cells were then washed twice and directly visualized using a laser scanning confocal microscope. A strong fluorescence signal was observed in the cytosol for cells incubated with the benzylated analogs, O^6-BnthG$_N$ and O^6-Bn^{tz}G$_N$, confirming their cellular uptake. No fluorescence signal was detected for the methylated analogs O^6-MethG$_N$ and O^6-Me^{tz}G$_N$ (Figure 4a).

Finally, to preliminarily evaluate the potential to utilize the benzylated surrogates for monitoring hAGT activity in real time in live cells, HEK293T cell cultures were incubated with either O^6-BnthG$_N$ (100 μM) or O^6-Bn^{tz}G$_N$ (250 μM) for 10 min and washed twice, and live-cell images were taken every 30 or 20 s, respectively, for 17 min. The fluorescence intensity decreased over time for both analogs (Figure 4b,c and Movies S1 and S2). This could correspond to the dealkylation reactions of O^6-BnthG$_N$ and O^6-Bn^{tz}G$_N$ to their respective G-surrogate nucleobases, which are much less emissive in the observed wavelengths (420−551 nm).[38] The change in fluorescence was quantified by measuring the mean fluorescence intensity in at least 10 different regions of interest (ROIs) over time (Figure 5). Decreases of 40 and 50% in fluorescence intensity of O^6-BnthG$_N$ and O^6-Bn^{tz}G$_N$, respectively, were seen (Figure 5a,b).

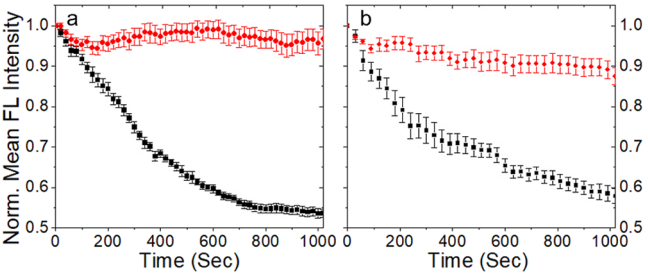

Figure 5. Real-time fluorescence monitoring of O^6-Bn^{tz}G$_N$ (a) and O^6-BnthG$_N$ (b) in live HEK293T (black) and CHO-K1 (red) cells. Data points are averages of fluorescence intensities measured over time from at least 10 ROIs and normalized.

The observed decrease in fluorescence could potentially stem from other unrelated photophysical processes, such as undesirable photobleaching, or cellular processes such as, but not limited to, metabolic degradation of the surrogates or their expulsion from the cells. To eliminate at least some of these alternative explanations for the time-dependent diminishing fluorescence, further experiments, within the scope of our laboratory, were performed. To exclude photobleaching, other areas of the wells that were not previously exposed to laser excitation were visualized after the 17 min imaging window. For both compounds, these later images displayed fluorescence intensities similar to the intensities of the images at the end of the imaging experiment (Figure S10), suggesting that the decrease in fluorescence occurs due to cellular processes and not photobleaching.

To further corroborate that hAGT is responsible for the decrease in fluorescence, real-time imaging experiments were repeated in CHO-K1 cells, which are known to be AGT-deficient.[16] Both O^6-BnthG$_N$ and O^6-Bn^{tz}G$_N$ displayed a fluorescent signal in the cytosol of CHO cells after a 10 min incubation, and indeed, no visual decrease in fluorescence intensities was observed for either of the tested analogs over time (Figure 4b,c and Movies S3 and S4). No to very little change (10%) in fluorescence was measured over time for O^6-Bn^{tz}G$_N$ and O^6-BnthG$_N$, respectively (Figure 5a,b), supporting that the change seen in the HEK293T cells occurs due to consumption of the analogs by hAGT.

CONCLUSIONS

In this study, we set out to design emissive probes capable of tracking the dealkylation reactions of hAGT. We synthesized the O6 methylated and benzylated derivatives of both the thiopheno- and isothiazolopyrimidine heterocyclic cores and established that the photophysical properties of the parent and alkylated nucleobases are distinct, allowing one to optically track the dealkylating reactions. By exposing both derivatives of each family to hAGT and the SNAP-Tag proteins, we established that the benzylated derivatives, O^6-BnthG$_N$ and O^6-Bn^{tz}G$_N$, provide a spectral window to monitor the reactions of these proteins and facilitate real-time measurements. Finally, our in vitro experiments in mammalian cells demonstrated that

https://doi.org/10.1021/acsomega.4c05700
ACS Omega 2024, 9, 36778−36786

O^6-BnthG$_N$ and O^6-Bn^{tz}G$_N$ are suitable for live-cell imaging. A continuous decrease in fluorescence intensity, observed in HEK293T but not in CHO-K1 cells, during real-time live-cell imaging monitoring experiments, suggested that the AGT reaction could be cellularly tracked. This system could potentially be further developed into a readily used assay in which the activity of hAGT in patients' specimens could be evaluated after incubation with such emissive nucleobase surrogates and provide a quantifiable measure of their cellular enzymatic dealkylation potency.

EXPERIMENTAL SECTION

General Chemistry Methods. Reagents, buffers, and salts were purchased from Sigma-Aldrich, Fluka, TCI, Acros, and Synchem, Inc. (Elk Grove, IL) and were used without further purification unless otherwise specified. Solvents were purchased from Sigma-Aldrich and Fisher Scientific and dried by standard techniques. NMR solvents were purchased from Cambridge Isotope Laboratories (Andover, MA). All reactions were monitored with analytical TLC (Merck Kieselgel 60 F_{254}). All experiments involving air- and/or moisture-sensitive compounds were carried out under an argon atmosphere. Column chromatography was carried out with a silica gel particle size of 40−63 μm. NMR spectra were obtained on a Varian Mercury 400 MHz. HPLC was performed using a Sepax Bio C-18 column (250 × 10 mm, 5 μm particle size) on an Agilent 1200 series HPLC system (Agilent Technologies). ESI-TOF mass spectra were obtained on an Agilent 6230 HR-ESI-TOF MS instrument at the Molecular Mass Spectrometry Facility at the UCSD Chemistry and Biochemistry Department.

Synthetic Procedures. Nucleobase analogs thG$_N$ and ^{tz}G$_N$ were synthesized based on previously reported procedures.[23,24,27]

4-(Benzyloxy)thieno[3,4-*d*]pyrimidin-2-amine (O^6-BnthG$_N$). To a flame-dried flask, purged with argon, solid thG$_N$ (0.040 g, 0.24 mmol) was added and dissolved in anhydrous DMF (3 mL). DBU (0.054 mL, 0.36 mmol) was then added dropwise followed by BOP (0.138 g, 0.31 mmol). The solution was allowed to stir at room temperature for 2.5 h, and then, 1 M NaOBn in BnOH (0.72 mL) was introduced dropwise. The reaction was allowed to stir overnight at room temperature and was then partitioned between DCM and water. The organic extract was washed twice with water and once with brine, dried over sodium sulfate, and evaporated to dryness. The resulting residue was subjected to column chromatography with a gradient of 0−5% MeOH in DCM to yield an off-white powder (0.040 g, 64%). ^{1}H NMR (400 MHz, DMSO-d_6): δ 8.28 (d, J = 3.2 Hz, 1H), 7.58−7.51 (m, 2H), 7.47−7.33 (m, 3H), 7.16 (d, J = 3.2 Hz, 1H), 6.95 (s, 2H), 5.55 (s, 2H). ^{13}C NMR (100 MHz, DMSO-d_6): δ 164.47, 159.37, 153.64, 148.73, 135.75, 128.29, 128.25, 128.11, 123.40, 117.63, 106.72, 66.53. ESI-HRMS calculated for $[C_{13}H_{12}N_3OS]^+$, 258.0696; found, 258.0697.

4-Methoxythieno[3,4-*d*]pyrimidin-2-amine (O^6-MethG$_N$). Solid thG$_N$ (0.040 g, 0.240 mmol) was placed in a flame-dried flask and dissolved in anhydrous DMF (3 mL). DBU (0.054 mL, 0.36 mmol) was then added dropwise followed by solid BOP (0.138 g, 0.311 mmol). The solution was stirred at room temperature for 2.5 h before 0.5 M NaOMe in MeOH (1.44 mL) was added dropwise. The reaction mixture was left to stir at room temperature overnight. The solution was then evaporated to dryness and subjected to column chromatography with a gradient of 0−10% MeOH in DCM, yielding an off-white powder (0.037 g, 86%). ^{1}H NMR (400 MHz, DMSO-d_6): δ 8.12 (s, 1H), 7.04 (s, 1H), 6.38 (s, 2H), 3.96 (s, 3H). ^{13}C NMR (100 MHz, DMSO-d_6): δ 164.31, 159.67, 153.71, 122,61, 107.66, 118.24, 54.01. ESI-HRMS calculated for $[C_7H_8N_3OS]^+$, 182.0383; found, 182.0383.

5-Aminoisothiazolo[4,3-*d*]pyrimidin-7(6*H*)-one (^{tz}G$_N$). Solid $DMSO_2$ (6 g, 9.25 mmol) was added to a flame-dried flask and heated to 125 °C. A homogeneous mixture of 4-aminoisothiazole-3-carboxamide hydrochloride salt (0.300 g, 1.54 mmol) and chloroformamidine hydrochloride (0.266 g, 2.31 mmol) was added in 2 batches, 15 min apart, to the liquid $DMSO_2$. The reaction was left to stir for 1.5 h and then cooled to room temperature. The solidified reaction mixture was then resuspended in a minimal amount of water, basified with concentrated ammonium hydroxide, and stirred vigorously for 1 h. The solution was then evaporated to dryness, resuspended in a minimal amount of DCM, filtered, and was then thoroughly washed with DCM. The remaining yellow solid was then dissolved in MeOH and evaporated to afford a light-yellow solid.

7-Methoxyisothiazolo[4,3-*d*]pyrimidin-5-amine (O^6-Me^{tz}G$_N$). To a flame-dried flask purged with argon were added solids ^{tz}G$_N$ (0.122 g, 0.725 mmol), DMAP (0.106 g, 0.870 mmol), and 2-mesitylenesulfonyl chloride (0.178 g, 1.09 mmol) and subsequently dissolved in anhydrous ACN (10 mL). DBU (0.16 mL, 1.09 mmol) was introduced dropwise, and the reaction mixture was left to stir overnight at room temperature. The suspension was filtered, and the solid was washed with ACN and diethyl ether. The orange-red solid was then dried under high vacuum for 2 h and then argon-purged. The solid was dissolved in anhydrous DMF (10 mL), and 0.5 M NaOMe in MeOH (4.36 mL) was added dropwise. After 30 min, the solution was partitioned between EtOAc and water. Brine was added to the aqueous phase, and the mixture was extracted with EtOAc twice more. The organic phases were combined, dried over sodium sulfate, and evaporated. The remaining residue was subjected to column chromatography with a gradient of 0−5% MeOH in DCM to afford a yellow solid (0.099 g, 75% yield). ^{1}H NMR (400 MHz, DMSO-d_6): δ 8.80 (s, 1H), 6.72 (s, 2H), 4.04 (s, 3H). ^{13}C NMR (100 MHz, DMSO-d_6): δ 162.11, 159.94, 153.39, 143.42, 136.49, 54.46. ESI-HRMS calculated for $[C_6H_7N_4OS]^+$, 183.0335; found, 183.0338.

7-(Benzyloxy)isothiazolo[4,3-*d*]pyrimidin-5-amine (O^6-Bn^{tz}G$_N$). Solids ^{tz}G$_N$ (0.052 g, 0.201 mmol), DMAP (0.030 g, 0.241 mmol), and 2-mesitylenesulfonyl chloride (0.066 g, 0.30 mmol) were added to a flame-dried flask purged with argon. The solids were then dissolved in anhydrous ACN (5 mL), and DBU (0.05 mL, 0.302 mmol) was dropwise introduced. The reaction mixture was stirred overnight at room temperature. The resulting suspension was filtered, and the filtrate was washed with acetonitrile and diethyl ether. The solid was then dried under high vacuum for 2 h, purged with argon, and dissolved in anhydrous DMF (5 mL). NaOBn (1 M) in BnOH (0.60 mL) was added dropwise to the solution. After 4 h, the solution was partitioned between DCM and water, and the aqueous layer was extracted with DCM twice more. The organic phases were combined, dried over sodium sulfate, and evaporated. The resulting residue was subjected to column chromatography with a gradient of 0−5%MeOH in DCM to afford a light-yellow solid (34 mg, 65%). ^{1}H NMR (400 MHz, DMSO-d_6): δ 8.80 (s, 1H), 7.54−7.58 (m, 2H),

https://doi.org/10.1021/acsomega.4c05700
ACS Omega 2024, 9, 36778−36786

7.35−7.45 (m, 3H), 6.76 (s, 2H), 5.54 (s, 2H). ^{13}C NMR (100 MHz, DMSO-d_6): δ 161.42, 159.86, 153.58, 143.32, 136.64, 136.28, 129.41, 129.05, 128.93, 68.39. ESI-HRMS calculated for $[C_{12}H_1N_4OS]^+$, 259.0648; found, 259.0644.

General Photophysical Methods. Absorption spectra were measured on a Shimadzu UV-2450 spectrometer setting the slit at 1 nm and with a 0.5 nm resolution. Emission spectra were measured on a Horiba Fluoromax-4, and measurements were taken with a 1 nm resolution and setting the slits to 1 nm. Emission intensities were corrected to reflect an optical density of 0.1 at the excitation wavelength. All measurements were carried out in a 3 mL 10 mm four-sided quartz cuvette purchased from Helma. Both instruments were equipped with a thermostat-controlled ethylene glycol-water bath, and all measurements were taken at 37.0 ± 0.1 °C. Measurements were recorded after a 3 min temperature equilibration period. All spectra were corrected for the blank.

Highly concentrated stocks solutions of $^{th}\mathbf{G}_N$, O^6-$\mathbf{Bn}^{th}\mathbf{G}_N$, O^6-$\mathbf{Me}^{th}\mathbf{G}_N$, $^{tz}\mathbf{G}_N$, O^6-$\mathbf{Bn}^{tz}\mathbf{G}_N$, and O^6-$\mathbf{Me}^{tz}\mathbf{G}_N$ were prepared in DMSO. Samples were prepared from the stock nucleobase solutions diluted to a total volume of 3 mL in deionized water or a DPBS buffer, mixed with a pipet for 10 s, and placed in the cuvette holder to equilibrate for 3 min. All samples contain 0.3 v/v % DMSO. All measurements were done in triplicate.

Quantum Yield Measurements. Fluorescence quantum yields were measured on a Horiba Fluoromax-4 with a 1 nm resolution, an excitation slit at 1 nm, and an emission slit at 3 nm. All sample concentrations were adjusted to have an optical density lower than 0.1 at the excitation wavelength. All measurements were done in triplicate. The fluorescence quantum yields were measured relative to 2-aminopurine (0.68 in water, λ_{ex} of 320 nm) as an external standard by using the following equation:

$$\phi = \phi_{STD}\frac{I}{I_{STD}}\frac{OD_{STD}}{OD}\frac{\eta^2}{\eta_{STD}^2}$$

where ϕ_{STD} is the fluorescence quantum yield of the standard, I and I_{STD} are the integrated area of the emission band of the sample and the standard, respectively, OD and OD_{STD} are the optical density at the excitation wavelength for the sample and the standard, respectively, and η and η_{STD} are the solvent refractive index of the sample and the standard solutions, respectively.

Protein Reaction: Real-Time Fluorescence Monitoring of hAGT and SNAP-Tag Reactions. Recombinant hAGT protein with a His-Tag terminus (MGMT; O-6-methylguanine-DNA methyltransferase) was purchased from BPS Bioscience, and SNAP-Tag purified protein with a C-terminal DDT moiety was purchased from New England Biolabs.

Reaction conditions were the same for all hAGT and SNAP-Tag reactions, as monitored by emission spectroscopy. Concentrated stocks were prepared in DMSO. Samples were prepared in a 125 μL of 10.00 mm four-sided quartz cuvette from Helma. Reactions had a total volume of 125 μL with a nucleobase concentration of 0.5 μM and a protein (either hAGT or SNAP-Tag) concentration of 2.5 μM in a 1× DPBS buffer. All measurements were taken at 37.0 ± 0.1 °C, and the protein was introduced after a 3 min temperature equilibration period. All samples contain 0.01 v/v% DMSO.

The protein-mediated conversion of emissive O^6-alkylguanine analogs was monitored by emission spectroscopy. Emission measurements were performed on a Horiba Fluoromax-4, collecting data every 150 s for at least 2550 s for O^6-$\mathbf{Me}^{th}\mathbf{G}_N$, O^6-$\mathbf{Bn}^{th}\mathbf{G}_N$, and O^6-$\mathbf{Me}^{tz}\mathbf{G}_N$, every 30 s for 2010 s for O^6-$\mathbf{Bn}^{tz}\mathbf{G}_N$ for the hAGT enzyme, every 150 s for 5100 s for O^6-$\mathbf{Me}^{th}\mathbf{G}_N$, O^6-$\mathbf{Bn}^{tz}\mathbf{G}_N$, and O^6-$\mathbf{Me}^{tz}\mathbf{G}_N$, and every 30 s for 1500 s for O^6-$\mathbf{Bn}^{th}\mathbf{G}_N$ for the SNAP-Tag enzyme. Real-time monitoring of the conversions was done upon excitation at the isosbestic point for each pair of compounds in a DPBS buffer. The conversions of O^6-$\mathbf{Bn}^{th}\mathbf{G}_N$ and O^6-$\mathbf{Me}^{th}\mathbf{G}_N$ to $^{th}\mathbf{G}_N$ were followed at 400 nm, with excitation at 321 and 325 nm, respectively, setting the excitation slit to 5 nm and the emission slit at 10 nm. The conversions of O^6-$\mathbf{Bn}^{tz}\mathbf{G}_N$ and O^6-$\mathbf{Me}^{tz}\mathbf{G}_N$ to $^{tz}\mathbf{G}_N$ were followed at 450 nm, with excitation at 334 nm for both compounds, setting the excitation slit at 1 nm and the emission slit at 10 nm. Each experiment was performed in triplicate. Note that there was a 6 s lag time after protein addition after time 0 measurement.

HPLC Monitoring of hAGT and SNAP-Tag Reactions. Reactions (total volume of 100 μL) with a nucleobase concentration of 4.3 μM and a protein (either hAGT or SNAP-Tag) concentration of 21.5 μM in a 1× DPBS buffer were performed at 37.0 °C. The protein was introduced after a 3 min temperature equilibration period, and the reaction was analyzed after 1500 s. For t = 0 s analysis, the reaction mixture and the protein were separately heated to 95 °C for 3 min and then mixed. The reaction mixtures were then centrifuged at 18,000g for 5 min and injected into an Agilent 1200 series HPLC system (Agilent Technologies). HPLC was performed using a Synergi 4 μm Fusion-RP 80 Å column (250 × 10 mm, 4 μm particle size) with a gradient of 0.5−60% ACN (0.1% formic acid) in H_2O (0.1% formic acid) for 30 min.

Mammalian Cell Culture. HEK293T cells were grown in DMEM, CHO-K1 cells were grown in DMEM/F12, and both media were supplemented with 10% FCS and 1% penicillin−streptomycin. All cells were grown in a humidified chamber of 95% air and 5% CO_2 at 37 °C.

Live-Cell Imaging. Microtiter plates (96-well) and FluoroDish wells used were coated with PDL before use according to the following procedure: Wells were covered with PDL solution (0.1 mg/mL, 100 or 120 μL per well for 96-well plates or FluoroDish wells, respectively) and incubated for 3 h at RT. The PDL solution was then removed by aspiration, and wells were resterilized under UV light for 20 min and further dried for an additional 1.5 h. Finally, wells were washed with PBS twice (100 or 120 μL per well).

Determination of Imaging Concentrations. HEK293T cells were plated into PDL-coated 96-well microtiter plates (30 × 10^3 cells per well) and allowed to adhere for 24 h. The medium was aspirated, and solutions of tested compounds in growth media (100 μL) were added at final concentrations of 100, 50, and 1 μM for O^6-$\mathbf{Me}^{th}\mathbf{G}_N$ and O^6-$\mathbf{Bn}^{th}\mathbf{G}_N$ and 500, 100, 50, and 1 μM for O^6-$\mathbf{Me}^{tz}\mathbf{G}_N$ and O^6-$\mathbf{Bn}^{tz}\mathbf{G}_N$. Cultures were then incubated for 1.5 h in a humidified chamber of 95% air and 5% CO_2 at 37 °C. Cells were then washed twice with a PBS buffer containing Ca and Mg ions and were visualized in this buffer using an EVOS widefield fluorescence microscope.

Confocal Microscopy. HEK293T cells were plated into PDL-coated FluoroDish wells of 10 mm diameter with a cover glass bottom (wpi), fit for live-cell imaging and compatible with oil objectives (100 × 10^3 cells per well), and allowed to adhere for 24 h. The medium was aspirated, and solutions of tested compounds in growth media (100 μL) were added at final concentrations of 500 μM of O^6-$\mathbf{Me}^{tz}\mathbf{G}_N$ and O^6-$\mathbf{Bn}^{tz}\mathbf{G}_N$

https://doi.org/10.1021/acsomega.4c05700
ACS Omega 2024, 9, 36778−36786

and 100 μM of O^6-MethG$_N$ and O^6-BnthG$_N$. Cultures were incubated for 1 h. During this incubation time, the nuclear stain NucRed Live 647 was added to 5−100 μL of culture and incubated for 30 min. Wells were then washed with PBS containing Ca, Mg, and 1 mM HEPES and were visualized in this buffer using a Nikon AXR confocal microscope with a four-line (405, 488, 561, and 640 nm) LUA-S4 laser engine and a DUX-VB detector using band-pass and long-pass filters for each channel (420−551 and 655−850 nm) mounted on a Nikon Ti2 using an Apo 100× 1.45 NA objective and operated using NIS-Elements 5.42.03 software. Image stacks were acquired in galvano mode in unidirectional scanning with a 405 nm laser at a 3% power and a 61.5 μm pinhole size and a 640 nm laser at a 2% power and a 61.0 μm pinhole size, at a frame size of 1024 × 1024 at a scan zoom of 1.7. Cells were maintained at 37 °C and 5% CO_2 with 80% humidity using an Okolab bold line. All images were taken at the same microscope settings.

Fluorescence Intensity Real-Time Monitoring of O^6-Bn-^{tz}G$_N$ and O^6-Bn-^{tz}G$_N$ in Live Cells. HEK293T or CHO-K1 cells were plated into PDL-coated FluoroDish wells (100×10^3 or 40×10^3, respectively) and allowed to adhere for 24 h. NucRed was added (5−100 μL) and incubated for 20 min. The medium was then aspirated, and solutions containing tested compounds and NucRed (5 μL) in media were added at final concentrations of 250 μM O^6-Bn^{tz}G$_N$ and 100 μM O^6-BnthG$_N$ and were incubated for 10 min. Wells were then aspirated and washed with FluoroBrite supplemented with 10% FCS and were visualized in this buffer using the same confocal microscope described above, in the same settings. Time lapse images were taken every 20 and 30 s for O^6-Bn^{tz}G$_N$ and O^6-BnthG$_N$, respectively, for 17 min. All images were taken at the same microscope settings. Mean fluorescence intensities of at least 10 different ROIs selected from the images as well as mean fluorescence intensities of the whole images were measured over time using ImageJ.

■ ASSOCIATED CONTENT

Supporting Information

The Supporting Information is available free of charge at https://pubs.acs.org/doi/10.1021/acsomega.4c05700.

Synthetic schemes, HPLC traces, crystal structures, widefield fluorescence microscopy calibration experiments, and comparison figure between before and after real-time live-cell imaging experiments (PDF)

Real-time live-cell imaging (Movie S1) (ZIP)

Real-time live-cell imaging (Movie S2) (ZIP)

Real-time live-cell imaging (Movie S3) (ZIP)

Real-time live-cell imaging (Movie S4) (ZIP)

■ AUTHOR INFORMATION

Corresponding Author

Yitzhak Tor − *Department of Chemistry and Biochemistry, University of California San Diego, La Jolla, California 92093-0358, United States;* orcid.org/0000-0003-3726-7799; Email: ytor@ucsd.edu

Authors

Kfir B. Steinbuch − *Department of Chemistry and Biochemistry, University of California San Diego, La Jolla, California 92093-0358, United States*

Marcela Bucardo − *Department of Chemistry and Biochemistry, University of California San Diego, La Jolla, California 92093-0358, United States*

Complete contact information is available at: https://pubs.acs.org/10.1021/acsomega.4c05700

Author Contributions

‡K.B.S. and M.B. contributed equally to this work.

Notes

The authors declare no competing financial interest.

■ ACKNOWLEDGMENTS

We thank the National Institutes of Health for generous support (through grant R35 GM139407), the UCSD Chemistry and Biochemistry Mass Spectrometry Facility, the UCSD NMR Facility, and the UCSD X-ray Crystallography Facility. Confocal microscopy was performed at the Nikon Imaging Center at UC San Diego. We thank R. Sanchez and P. Guo for their support. We thank Dr. K. Hadidi for fruitful discussions.

■ ABBREVIATIONS

hAGT, human O^6-alkylguanine-DNA-transferase; thN, thieno-[3,4-*d*]pyrimidine; ^{tz}N, isothiazolo[4,3-*d*]pyrimidine; ROI, region of interest; BOP, benzotriazole-1-yloxytris-(dimethylamino)phosphonium hexafluorophosphate; DBU, 1,8-diazabicyclo[5.4.0]undec-7-ene; DMAP, 4-dimethylamino-pyridine; TLC, thin-layer chromatography

■ REFERENCES

(1) Fahrer, J.; Christmann, M. DNA Alkylation Damage by Nitrosamines and Relevant DNA Repair Pathways. *Int. J. Mol. Sci.* **2023**, *24*, 4684.

(2) De Bont, R.; van Larebeke, N. Endogenous DNA Damage in Humans: A Review of Quantitative Data. *Mutagenesis* **2004**, *19* (3), 169−185.

(3) Shrivastav, N.; Li, D.; Essigmann, J. M. Chemical Biology of Mutagenesis and DNA Repair: Cellular Responses to DNA Alkylation. *Carcinogenesis* **2010**, *31* (1), 59−70.

(4) Mingard, C.; Wu, J.; McKeague, M.; Sturla, S. J. Next-Generation DNA Damage Sequencing. *Chem. Soc. Rev.* **2020**, *49* (20), 7354−7377.

(5) Pegg, A. E. Enzymatic Removal of O6-Methylguanine From DNA by Mammalian Cell Extracts. *Biochem. Biophys. Res. Commun.* **1978**, *84* (1), 166−173.

(6) Yarosh, D. B.; Rice, M.; Day, R. S.; Foote, R. S.; Mitra, S. O6-Methylguanine-DNA Methyltransferase in Human Cells. *Mutat. Res. DNA Repair Reports* **1984**, *131* (1), 27−36.

(7) Pegg, A. E.; Byers, T. L.; Swenn, K.; Boosalis, M.; Samson, L.; Moschel, R. C.; Dolan, M. E. Mechanism of Inactivation of Human O6-Alkylguanine-DNA Alkyltransferase by O6-Benzylguanine. *Biochemistry* **1993**, *32* (45), 11998−12006.

(8) Xu-Welliver, M.; Pegg, A. E. Degradation of the Alkylated Form of the DNA Repair Protein, O6-Alkylguanine-DNA Alkyltransferase. *Carcinogenesis* **2002**, *23* (5), 823−830.

(9) Sharma, S.; Salehi, F.; Scheithauer, B. W.; Rotondo, F.; Syro, L. V.; Kovacs, K. Role of MGMT in Tumor Development, Progression, Diagnosis, Treatment and Prognosis. *Anticancer Res.* **2009**, *29* (10), 3759−3768.

(10) Wickström, M.; Dyberg, C.; Milosevic, J.; Einvik, C.; Calero, R.; Sveinbjörnsson, B.; Sandén, E.; Darabi, A.; Siesjö, P.; Kool, M.; Kogner, P.; Baryawno, N.; Johnsen, J. I. Wnt/β-Catenin Pathway Regulates MGMT Gene Expression in Cancer and Inhibition of Wnt Signalling Prevents Chemoresistance. *Nat. Commun.* **2015**, *6*, 8904.

(11) Gerson, S. L. MGMT: Its Role in Cancer Aetiology and Cancer Therapeutics. *Nat. Rev. Cancer* **2004**, *4* (4), 296−307.
(12) Singh, N.; Miner, A.; Hennis, L.; Mittal, S. Mechanisms of Temozolomide Resistance in Glioblastoma - a Comprehensive Review. *Cancer Drug Resist.* **2020**, *4* (1), 17−43.
(13) Trivedi, R. N.; Almeida, K. H.; Fornsaglio, J. L.; Schamus, S.; Sobol, R. W. The Role of Base Excision Repair in the Sensitivity and Resistance to Temozolomide-Mediated Cell Death. *Cancer Res.* **2005**, *65* (14), 6394−6400.
(14) Liu, M.; Yu, W.; Yang, X.; Li, Y.; Zhang, Y.; Zhang, C. A Simple and Rapid Mix-and-Read Assay for Sensitive Detection of O6-Methylguanine DNA Methyltransferase. *Chem. Commun.* **2022**, *58*, 8662−8665.
(15) Fillion, A.; Franco Pinto, J.; Granzhan, A. Harnessing an Emissive Guanine Surrogate to Design Small-Molecule Fluorescent Chemosensors of O 6-Methylguanine-DNA-Methyltransferase (MGMT). *Org. Biomol. Chem.* **2022**, *20* (9), 1888−1892.
(16) Yu, W. T.; Wu, T. W.; Huang, C. L.; Chen, I. C.; Tan, K. T. Protein Sensing in Living Cells by Molecular Rotor-Based Fluorescence-Switchable Chemical Probes. *Chem. Sci.* **2016**, *7* (1), 301−307.
(17) Moser, A. M.; Patel, M.; Yoo, H.; Balis, F. M.; Hawkins, M. E. Real-Time Fluorescence Assay for O6-Alkylguanine-DNA Alkyltransferase. *Anal. Biochem.* **2000**, *281* (2), 216−222.
(18) Ayan, S.; Rotaru, A. M.; Kaye, E. G.; Juneau, G.; Das, S.; Wilds, C. J.; Beharry, A. A. A Chloromethyl-Triazole Fluorescent Chemosensor for O6-Methylguanine DNA Methyltransferase. *Org. Biomol. Chem.* **2024**, *22* (14), 2749−2753.
(19) Han, Y.; Li, D. L.; Han, Q.; Ma, F.; Zhang, C. Y. Integration of Demethylation-Activated DNAzyme with a Single Quantum Dot Nanosensor for Sensitive Detection of O6-Methylguanine DNA Methyltransferase in Breast Tissues. *Anal. Chem.* **2024**, *96* (11), 4487−4494.
(20) Juillerat, A.; Gronemeyer, T.; Keppler, A.; Gendreizig, S.; Pick, H.; Vogel, H.; Johnsson, K. Directed Evolution of O 6 -Alkylguanine-DNA Alkyltransferase for Efficient Labeling of Fusion Proteins with Small Molecules In Vivo. *Chem. Biol.* **2003**, *10*, 313−317.
(21) Keppler, A.; Pick, H.; Arrivoli, C.; Vogel, H.; Johnsson, K. Labeling of Fusion Proteins with Synthetic Fluorophores in Live Cells. *Proc. Natl. Acad. Sci. U. S. A.* **2004**, *101* (27), 9955−9959.
(22) Juillerat, A.; Heinis, C.; Sielaff, I.; Barnikow, J.; Jaccard, H.; Kunz, B.; Terskikh, A.; Johnsson, K. Engineering Substrate Specificity of O 6 - Alkylguanine-DNA Alkyltransferase for Specific Protein Labeling in Living Cells. *ChemBioChem* **2005**, *6*, 1263−1269.
(23) Shin, D.; Sinkeldam, R. W.; Tor, Y. Emissive RNA Alphabet. *J. Am. Chem. Soc.* **2011**, *133* (38), 14912−14915.
(24) Rovira, A. R.; Fin, A.; Tor, Y. Chemical Mutagenesis of an Emissive RNA Alphabet. *J. Am. Chem. Soc.* **2015**, *137* (46), 14602−14605.
(25) Steinbuch, K. B.; Tor, Y. Isomorphic Fluorescent Nucleoside Analogs. In *Handbook of Chemical Biology of Nucleic Acids*; Sugimoto, N., Ed.; Springer Nature Singapore: Singapore, 2023.
(26) Tor, Y. Isomorphic Fluorescent Nucleosides. *Acc. Chem. Res.* **2024**, *57*, 1325−1335.
(27) Bucardo, M. S.; Wu, Y.; Ludford, P. T.; Li, Y.; Fin, A.; Tor, Y. Real-Time Monitoring of Human Guanine Deaminase Activity by an Emissive Guanine Analog. *ACS Chem. Biol.* **2021**, *16* (7), 1208−1214.
(28) Gewald, K.; Bellmann, P. Synthese Und Reaktionen von 4-Aminoisothiazolen. *Liebigs Ann. Chem.* **1979**, *1979*, 1534−1546.
(29) McManus, F. P.; Fang, Q.; Booth, J. D. M.; Noronha, A. M.; Pegg, A. E.; Wilds, C. J. Synthesis and Characterization of an O6−2′-Deoxyguanosine- Alkyl-O6−2′-Deoxyguanosine Interstrand Cross-Link in a 5′-GNC Motif and Repair by Human O6-Alkylguanine-DNA Alkyltransferase. *Org. Biomol. Chem.* **2010**, *8* (19), 4414−4426.
(30) Lakshman, M. K.; Frank, J. A Simple Method for C-6 Modification of Guanine Nucleosides. *Org. Biomol. Chem.* **2009**, *7* (14), 2933−2940.
(31) Sholokh, M.; Improta, R.; Mori, M.; Sharma, R.; Kenfack, C.; Shin, D.; Voltz, K.; Stote, R. H.; Zaporozhets, O. A.; Botta, M.; Tor, Y.; Mély, Y. Tautomers of a Fluorescent G Surrogate and Their Distinct Photophysics Provide Additional Information Channels. *Angew. Chemie - Int. Ed.* **2016**, *55* (28), 7974−7978.
(32) Mollwitz, B.; Brunk, E.; Schmitt, S.; Pojer, F.; Bannwarth, M.; Schiltz, M.; Rothlisberger, U.; Johnsson, K. Directed Evolution of the Suicide Protein O 6-Alkylguanine-DNA Alkyltransferase for Increased Reactivity Results in an Alkylated Protein with Exceptional Stability. *Biochemistry* **2012**, *51* (5), 986−994.
(33) Daniels, D. S.; Tainer, J. A. Conserved Structural Motifs Governing the Stoichiometric Repair of Alkylated DNA by O6-Alkylguanine-DNA Alkyltransferase. *Mutat. Res. - DNA Repair* **2000**, *460* (3−4), 151−163.
(34) Wibley, J. E. A.; Pegg, A. E.; Moody, P. C. E. Crystal Structure of the Human O6-Alkylguanine-DNA Alkyltransferase. *Nucleic Acids Res.* **2000**, *28* (2), 393−401.
(35) Goodtzova, K.; Kanugula, S.; Edara, S.; Pegg, A. E. Investigation of the Role of Tyrosine-114 in the Activity of Human O6- Alkylguanine-DNA Alkyltranferase. *Biochemistry* **1998**, *37* (36), 12489−12495.
(36) Vora, R. A.; Pegg, A. E.; Ealick, S. E. A New Model for How O6-Methylguanine-DNA Methyltransferase Binds DNA. *Proteins Struct. Funct. Genet.* **1998**, *32* (1), 3−6.
(37) Imal, Y.; Oda, H.; Nakatsuru, Y.; Ishikawa, T. A Polymorphism at Codon 160 of Human o Methylguanine-DNA Methyltransferase Gene in Young Patients with Adult Type Cancers and Functional Assay. *Carcinogenesis* **1995**, *16* (10), 2441−2445.
(38) Both $^{th}\mathbf{G}_N$ and $^{tz}\mathbf{G}_N$ have minimal absorbance at 405 nm, the fluorescence microscope's wavelength used for excitation of $\boldsymbol{O^6}$-$\mathbf{Bn}^{th}\mathbf{G}_N$ and $\boldsymbol{O^6}$-$\mathbf{Bn}^{tz}\mathbf{G}_N$. The dealkylation reaction products, $^{th}\mathbf{G}_N$ and $^{tz}\mathbf{G}_N$, are therefore not expected to be visible in the cells at the microscope's settings used to visualize the alkylated surrogates. A decrease in microscopy-detected fluorescence is therefore expected for both dealkylation reactions, despite the similar quantum yields of $\boldsymbol{O^6}$-$\mathbf{Bn}^{th}\mathbf{G}_N$ and $^{th}\mathbf{G}_N$.

https://doi.org/10.1021/acsomega.4c05700
ACS Omega 2024, 9, 36778−36786